International Journal of Coal Geology 191 (2018) 125–134

Contents lists available at ScienceDirect

International Journal of Coal Geology

journal homepage: www.elsevier.com/locate/coal

Oil expulsion in marine shale and its influence on the evolution of nanopores during semi-closed pyrolysis

Liangliang Wu[a,*], Ansong Geng[a], Peng Wang[b]

[a] The State Key Laboratory of Organic Geochemistry, Guangzhou Institute of Geochemistry, Chinese Academy of Sciences, Wushan, Guangzhou 510640, PR China
[b] Henan Province Development and Reform Commission, Zhengzhou 450018, PR China

ARTICLE INFO

Keywords:
Oil expulsion
Evolution of nanopores
Semi-closed pyrolysis
Gas adsorption measurement

ABSTRACT

Oil expulsion is an important process for the evolution of shale, especially in the oil-generative window. Low oil expulsion efficiency will cause the retention of oil and gas in mature source rock. This study used semi-closed pyrolysis to simulate the hydrocarbon generation and expulsion process of the Xiamaling Formation marine shale at various conditions. Low-pressure nitrogen (N_2) and carbon dioxide (CO_2) gas adsorption isotherms were obtained for the original shale sample and its thermally evolved solid residues. The results showed that the amount of residual bitumen first increased with increasing expulsion efficiency (EE < 13.43%) and then remained constant with a further increase in EE. This finding implied that the saturation threshold for the source rock must be reached before oil expulsion can proceed. Meanwhile, the evolution of pore volumes with EE can be divided into two stages. The pore volumes decreased sharply in the first stage (EE < 13.43%), whereas they decreased slowly in the second stage (EE > 13.43%). The evolution of volume for micropores and fine mesopores with EE is very similar to that of expelled hydrocarbons. This similar evolution trend was further confirmed by the abovementioned oil expulsion model. This study enhanced understanding of the generation and evolution of shale gas in the oil-generative window.

1. Introduction

Conventional oil and gas are the most important energy sources in the world. Currently, however, unconventional gas is attracting much attention due to the growing energy demand and the great success of the North America shale gas revolution in recent decades (Curtis, 2002; Montgomery et al., 2005; Jarvie et al., 2007; Pollastro, 2007; Dai et al., 2017). Significant breakthroughs have also been obtained in recent evaluations and explorations of shale gas in China (Chen et al., 2011; Sun et al., 2012; Wang et al., 2013; Tan et al., 2014; Zou et al., 2015). Compared to traditional natural gas reservoirs, shale is generally characterized by low porosity and permeability. Additionally, shale gas production depends on the ability of pore systems to store and release hydrocarbon gas (Ross and Bustin, 2007, 2008; Wu et al., 2012; Cao et al., 2015). Thus, pore characterization is very important for the evaluation of shale gas.

The evolution of shale pore structure is very complicated, with a great number of geological factors controlling such processes, such as total organic carbon (TOC), thermal maturity, burial depth and mineralogy (Mastalerz et al., 2008; Loucks et al., 2009; Modica and Lapierre, 2012; Valenza et al., 2013; Suárez-Ruiz et al., 2016). Thermal maturity is considered the main factor, at least to a large extent, that controls the porosity in organic matter (Loucks et al., 2009; Modica and Lapierre, 2012; Valenza et al., 2013). Many previous studies have focused on the thermal maturity of shale based on the results from both natural maturity sequences (Mastalerz et al., 2013; Wei et al., 2014; Mathia et al., 2016) and artificial thermal simulation experiments (Chen and Xiao, 2014; Tang et al., 2015; Sun et al., 2015; Liu et al., 2017). However, there is no agreement on the evolution of nanopores in shale during thermal maturation. It is probably because of source rock heterogeneity for many factors, such as mineral composition, TOC, the type of organic matter, diagenesis and maturity (Sun et al., 2015). Recently, Mathia et al. (2016) suggested that the evolution of nanoporosity in natural shale is a comprehensive function of multiple factors including (1) the primary shale composition; (2) carbonate diagenesis; (3) compaction (pressure); and (4) the maturation (temperature), micro-migration, local trapping and gasification of heterogeneous organic phases. Therefore, studies of the comprehensive effects of multiple factors may provide more reasonable explanations for the evolution of nanoporosity in natural shale.

Oil expulsion is considered the initial step in the release of generated petroleum compounds from kerogen into the adjacent reservoir or

* Corresponding author.
E-mail address: wuliangliang@gig.ac.cn (L. Wu).

https://doi.org/10.1016/j.coal.2018.04.001
Received 7 December 2017; Received in revised form 30 March 2018; Accepted 1 April 2018
Available online 03 April 2018

migration layer through capillaries and narrow pores of a fine-grain source rock (Tissot and Welte, 1984). It is an important process for the evolution of shale, especially in the oil-generative window in which the endured temperature and pressure are not very high. The process of oil expulsion is closely related to pore structure evolution during kerogen maturation (Sun et al., 2015). Namely, high porosity occurring in the mature source rock will promote oil expulsion, whereas low porosity will prohibit oil expulsion. For most commercial shale gas plays, their oil expulsion efficiency is very low due to the low porosity and permeability (Jarvie, 2012). The most pronounced changes in the physical and chemical conditions during natural oil generation and expulsion are the increase in temperature and pressure (Tissot and Welte, 1984). This implies that the oil expulsion efficiency of shale is a comprehensive result of the changes in temperature and pressure. Meanwhile, compaction (pressure) and maturation (temperature) are two important factors for the evolution of nanoporosity in natural shale (Mathia et al., 2016). Thus, studying the oil expulsion influence on nanopore evolution will enhance our understanding of the combined influences of maturity and pressure on the evolution of nanoporosity in natural shale.

This study chose semi-open pyrolysis at temperatures of 300 °C to 370 °C for 72 h (Easy %Ro: 0.7%–1.3%) to investigate the oil expulsion process and evolution of nanopores during the oil-generative window. Most of the shale gas strata in the Sichuan Basin experienced a deep burial of 3–5 km (Liu et al., 2009; Ma et al., 2008; Zhang et al., 2008; Xiao et al., 2013), with a high pressure coefficient of 1.3–2.1 (Zou et al., 2015). Given a normal hydrostatic pressure increase of 10 MPa/km, most of the shale gas strata in the Sichuan Basin experienced a hydrostatic pressure of approximately 40–100 MPa. Thus, a pressure of 50–100 MPa was used in this study, because this range covered most of the conditions of the evolution of shale in Sichuan Basin. Subsequently, the evolution of nanopores in the simulated sequence was analyzed through gas adsorption methods, which have the advantages of convenient operation, maintaining the natural pore characteristics, and the ability to assess the complete nanopore size range (Zhang et al., 2017). The aim of this study is to reveal the oil expulsion process of shale and its influence on the evolution of nanopore systems.

2. Samples and methods

2.1. Samples

The investigated oil shale was sampled from the outcrop of the Xiamaling Formation in the Xiahuanyuan area of Jixian in Tianjing, China. The sample is immature, with a Ro value of 0.6%. The basic petrological and geochemical parameters are presented in Table 1. The sample is organic-rich, with a total organic carbon (TOC) content of 5.39%. Rock-Eval analysis revealed this oil shale to have a Tmax of 434 °C and a HI value of 564 mg/g TOC. The kerogen is type II (Liu et al., 1990; Xie et al., 2013). Minerals in the oil shale include quartz (51.4%), illite (26.4%), albite (10.3%), magnesian calcite (2.6%), and amorphous stuff (9.3%).

2.2. Pyrolysis experiment

This study used semi-closed pyrolysis, which was used to study oil generation (Lu, 1990), to artificially simulate the hydrocarbon generation and expulsion process. A schematic diagram of a high pressure, semi-closed pyrolysis system was shown by Liu et al. (2017). First, the oil shale sample was crushed into ≤80 mesh (180 μm) powder. Then, the crushed oil shale powder was loaded into a stainless steel cylinder (5 cm o.d. (outer diameter) 3 cm i.d. (inner diameter)) and sealed on both sides. The sealed cylinders were then compacted by a jack under vertical pressures of 50, 75, and 100 MPa, respectively. The cylinders were heated in an oven to 300 °C, 343 °C, and 370 °C and then held for 72 h, respectively. The calculated vitrinite reflectances from the Easy % Ro method (Sweeney and Burnham, 1990) for the kerogen heated to 300 °C, 343 °C, and 370 °C for 72 h were 0.7%, 1.0%, and 1.3%, respectively (in the oil-generative window). After cooling, the sealed cylinders were removed to collect the pyrolyzed products (expelled liquid oil and gas). The expelled oil and gas during the pyrolysis experiment were collected and analyzed. Finally, the pyrolyzed sample was Soxhlet extracted with dichloromethane: methanol (93,7 v:v) for 72 h to obtain the retained hydrocarbon (residual bitumen).

2.3. Methods

2.3.1. Gas composition analysis

The generated hydrocarbon gas was directly injected by a gas-tight syringe from the collecting tube into a customized vacuum line connected to an Agilent 6890 N capillary gas chromatograph modified by Wasson ECE Instrumentation for determination of molecular composition. A Poraplot Q capillary column (30 m × 0.25 mm × 0.25 μm) was used with helium as a carrier gas. The GC oven was held isothermally at 70 °C for 6 mins, programmed to increase to 180 °C at a rate of 15 °C/min and held for 4 min. Gaseous hydrocarbons (C_{1-5}) were quantified by using an external standard. The sum of the expelled hydrocarbon gases for each pyrolysis is shown in Table 2. The relative error is < 0.5% for this method (Pan et al., 2012; Jin et al., 2013).

2.3.2. Pore structure distributions (PSD)

Low-pressure nitrogen (N_2) and carbon dioxide (CO_2) gas adsorption isotherms were conducted on a Micromeritics ASAP-2460 Accelerated Surface Area and Porosimetry System. The pyrolyzed samples were all analyzed before and after Soxhlet extraction using dichloroform (DCM) for 72 h. The samples were crushed to 60–120 mesh size (250–125 μm) and degassed at 110 °C for 12 h in a vacuum chamber prior to analysis to remove the residual volatile material and free water. Nitrogen isotherms at 77 K were collected within a relative pressure (p/p^0) range of 0.005–0.998 (p is the balance pressure, and p^0 is the saturation pressure). Carbon dioxide isotherms were collected at 273.15 K at relative pressures of 0.00006–0.03.

The pore size distributions (PSDs) of the investigated samples were obtained using the composited N_2 and CO_2 non-local-density functional theory (NLDFT) method based on adsorption isotherms (Wei et al., 2016). This method enables the most suitable detection range (0.33–100 nm) and has high reliability and accuracy. As the maximum pore diameter calculated by NLDFT is 100 nm, the NLDFT analysis based on N_2 and CO_2 composited adsorption isotherms is used here to investigate the characteristics of pores with diameters (D) up to 100 nm. To better understand their evolution, the nanopores were subdivided into micropores (D < 2 nm), fine mesopores (2 < D < 10 nm), medium mesopores (10 < D < 25 nm), coarse mesopores (25 < D < 50 nm), and macropores (D > 50 nm), according to the IUPAC classification (Thommes et al., 2015) and previous work (Chalmers et al., 2012).

Table 1
The basic geochemical parameters of the investigated sample.

Sample	Lithology	Kerogen	TOC (%)	S1 (mg/g source rock)	S2 (mg/g source rock)	Tmax (°C)	HI	Ro (%)	$\delta^{13}C$ (‰)
XML	Calcareous shale	II_1 sapropelic	5.39	1.84	42.56	434	564	0.6	−30.97

Table 2
The TOC normalized yields of residual bitumen, expelled hydrocarbons, total generated hydrocarbons and the expulsion efficiency for semi-closed pyrolysis runs at various conditions.

Temperature (°C)	Pressure (MPa)	Total yield (mg/gTOC)	Residual bitumen (mg/g TOC)	Expelled hydrocarbon (mg/gTOC)			Expulsion efficiency (%)
				Liquid	Gas	Total	
300	50	38.94	35.24	3.01	0.70	3.71	9.52
	75	34.64	32.05	2.33	0.26	2.59	7.47
	100	37.69	35.1	2.56	0.04	2.60	6.89
343	50	75.76	65.59	6.91	3.26	10.17	13.43
	75	60.29	56.01	3.30	0.97	4.27	7.09
	100	59.47	56.16	3.05	0.26	3.31	5.57
370	50	110.01	67.85	37.35	4.82	42.17	38.33
	75	90.58	70.59	18.68	1.31	19.99	22.07
	100	84.34	65.31	18.36	0.66	19.02	22.56

Note: expulsion efficiency was calculated by the amount of expelled hydrocarbon divided by the total yield.

3. Results

3.1. The yield of semi-closed pyrolysis

The TOC normalized amounts of total generated liquid hydrocarbons, total generated gas, and the retained liquid hydrocarbons within shales were all determined and are shown in Table 2. The amount of total yield for a certain pyrolysis was obtained by the sum of its residual hydrocarbon and its expelled hydrocarbons (including both liquid and gas products). Meanwhile, expulsion efficiency was calculated by the amount of expelled hydrocarbon divided by the total yield. At the same temperature, increasing pressure seemed to inhibit the generation and expulsion of oil (Michels and Landais, 1994). For example, when the temperature was 370 °C, the total hydrocarbon yield was reduced from 110.01 mg/g TOC at 50 MPa to 84.34 mg/g TOC at 100 MPa, and the expelled hydrocarbons were reduced from 37.35 mg/g TOC at 50 MPa to 18.36 mg/g TOC at 100 MPa. However, the residual bitumen seemed to be relatively constant with increasing pressure when the temperature exceeded 343 °C. Conversely, an increasing temperature seemed to promote the generation and expulsion of oil (Table 2). When the pressure was 50 MPa, the total hydrocarbon yield increased gradually from 38.94 mg/g TOC at 300 °C to 110.01 mg/g TOC at 370 °C.

3.2. Adsorption isotherms

The pore size distributions of the original shale and its thermally evolved solid residues (residue from the artificial thermal evolution) after extraction were characterized using the combination of low-pressure N_2 and CO_2 adsorption methods. The nitrogen isotherms at 77.35 K for the original kerogen and its thermally evolved solid residues are presented in Fig. 1. All the isotherms show a hysteresis pattern without a plateau at higher pressures, mainly corresponding to Type IV, as defined by the IUPAC (Thommes et al., 2015). This result implies that the samples contain both mesopores and macropores (Sing et al., 1985). The large adsorption amount at low relative pressure ($p/p^0 < 0.01$) in the original sample indicates the presence of micropores. However, the adsorption amount at a low relative pressure ($p/p^0 < 0.01$) in the thermally evolved solid residue is sharply reduced because of the pressure and temperature increase. The isotherms also show forced closure of the desorption branch at $p/p^0 \approx 0.45$, which was referred to as the "Tensile Strength Effect" (Groen et al., 2003). The phenomenon of the "Tensile Strength Effect" was also identified by Suárez-Ruiz et al. (2016) in Cretaceous shale oil. According to a study of porosity in carbon materials, Groen et al. (2003) believe the "Tensile Strength Effect" is a result of hemispherical meniscus instability during desorption in pores with critical diameters of approximately 4 nm. Additionally, all the adsorption amounts increased without limit when $p/p^0 = 1$, which is an indicator of macropores. The Type IV isotherm is characterized by a hysteresis loop associated with capillary condensation in the mesopore structure. The loop was close to type H2 for the original kerogen, implying the presence of ink bottle pores. In contrast, the loop was close to type H4 for the thermal simulated residue, indicating material composed of narrow slots (Thommes et al., 2015). It seemed the ink bottle pores in the original kerogen were compacted into narrow slots.

Fig. 2 gives an overview of the carbon dioxide isotherms for the original sample and its pyrolytic residues, and it corresponds to a Type I isotherm given by microporous solids (Thommes et al., 2015). The adsorbed amounts at maximum relative pressure (p/p^0 of 0.03) for all samples range from 1.10 cm^3/g to 1.88 cm^3/g (Fig. 2). However, such maximum adsorption amounts cannot be directly used to represent the real micropore volume because the maximum equilibrium pressure used in this study (1 bar) was far lower than the CO_2 saturation pressure (34.5 bar) at 273 K (Tian et al., 2015). The above N_2 and CO_2 isotherms indicate that the original shale and its thermally simulated residues possess complex pore structures, with pore sizes ranging from micropores to macropores.

3.3. Pore size distribution

The combination N_2 and CO_2 adsorption data based on the NLDFT theory was used to reflect the pore size distribution (PSD) of the investigated samples (Wei et al., 2016). The PSD of the non-extracted shale simulation series is shown in Fig. 3. It is clear that temperature is an important factor that controls the PSD of the non-extracted shale samples. The non-extracted shale simulation series exhibit a bimodal PSD, with the dominant pores being micropores and mesopores. At the same pressure, the nanopores with diameters of 0–10 nm were gradually reduced with rising temperature (Fig. 3). Fig. 4 shows the PSD of the artificially evolved shales after extraction. The extracted sample (Fig. 4) appeared to show a similar PSD to the corresponding non-extracted original sample (Fig. 3). However, the S_{NLDFT} and V_{NLDFT} for the extracted pyrolytic shales increased obviously compared to those of corresponding non-extracted samples (Table 3). The V_{NLDFT} was in the range of 12.32 m^2/g to 18.13 m^2/g for non-extracted samples, whereas it was in the range of 12.53 m^2/g to 24.68 m^2/g for extracted samples (Table 3).

4. Discussion

4.1. The process of oil expulsion

Fig. 5 shows the varying trends of the total hydrocarbon yield, the amount of residual bitumen, and the amount of expelled hydrocarbons with increasing EE. The expulsion efficiencies (EE) for all the pyrolysis runs were calculated using the amount of expelled hydrocarbons (liquid hydrocarbons plus gas) divided by the total hydrocarbon yield

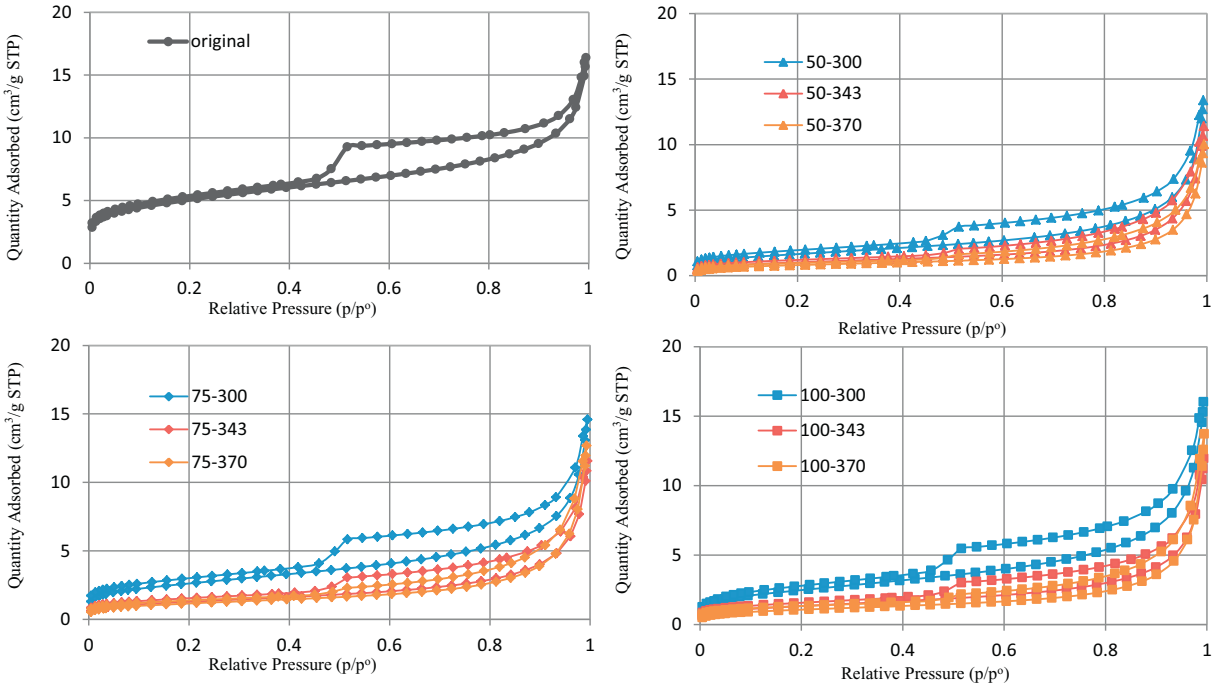

Fig. 1. N_2 gas adsorption and desorption isotherms at 77 K for the original shale and its thermally evolved solid residues at various conditions.

(Table 2). The amount of generated hydrocarbon was lower than 60 mg/g TOC when EE was < 10%, and it increased from 59.47 mg/g TOC at EE of 5.57% to 110.01 mg/g TOC at EE of 38.33%. This result implies that hydrocarbon generation promotes oil expulsion. However, the amount of residual bitumen showed a quite different evolution trend compared to those of the total hydrocarbon yield and the amount of expelled hydrocarbons. It first increased with increasing EE (EE < 13.43%), and then remained constant with a further increase in EE (EE > 13.43%). It was suggested that the expulsion of oil after its generation from the cracking of kerogen is controlled by absorption (physical) or adsorption (chemical) of the hydrocarbon products onto the kerogen surface and/or diffusion through the kerogen (Stainforth and Reinders, 1990; Thomas and Clouse, 1990a, 1990b, 1990c; Sandvik et al., 1992; Pepper and Corvi, 1995; Ritter, 2003). Such expulsion models suggest that the generated oil first absorbed or adsorbed into the macrostructure of kerogen and was then expelled from the source rock to the reservoir when the amount exceeded the maximum hydrocarbon sorption capacity (saturation threshold). The data in this study indeed confirmed the above expulsion models (Fig. 5 and Table 2). In this study, the amount of expelled hydrocarbon was very small at first, and it significantly increased when the total yield of generated hydrocarbon exceeds the value of 65 mg/g TOC (Fig. 5). Thus, it seems the saturation threshold for the investigated shale was about 65 mg/g TOC.

4.2. The distribution of retained hydrocarbon occupied places in shale

Generally, the oil expulsion efficiency in geological conditions cannot reach 100%. Namely, the existence of retained hydrocarbon in the source rock is inevitable. Recently, the effect of pore clogging in geological samples (shale or coal) by retained hydrocarbon (oil/bitumen) was reported by many researchers through comparisons of shale or coal pores before and after solvent extraction (e.g., Furmann et al., 2013; Valenza et al., 2013; Wei et al., 2014; Zargari et al., 2015; Zhang

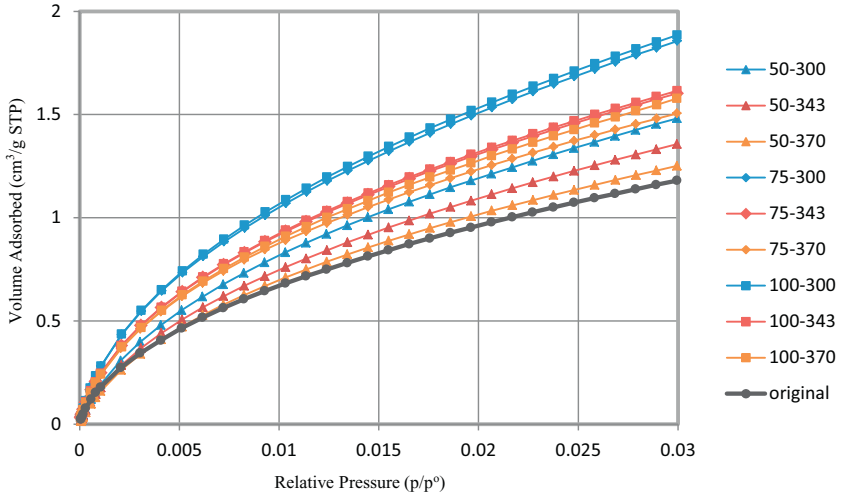

Fig. 2. CO_2 gas adsorption isotherms at 273 K for the original shale and its thermally evolved solid residues at various conditions.

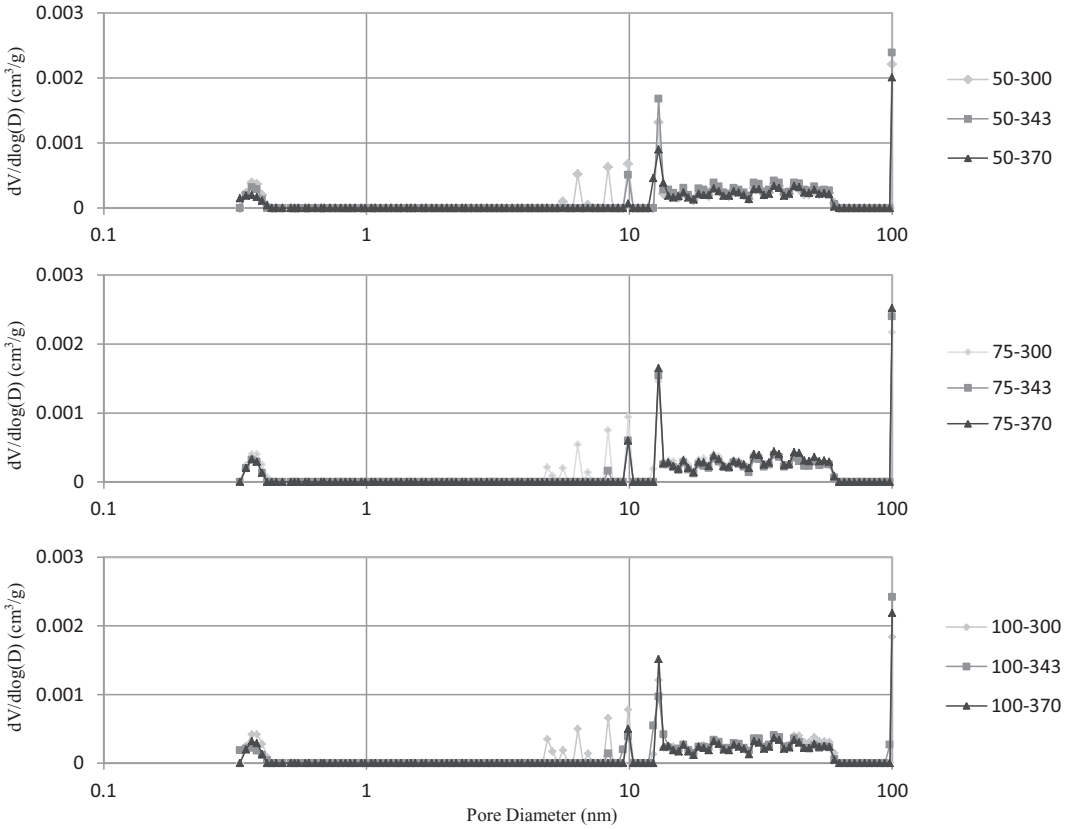

Fig. 3. Plot of dV/dlog(W) versus Pore diameter for the thermally evolved solid residues of the investigated shale before extration at various conditions.

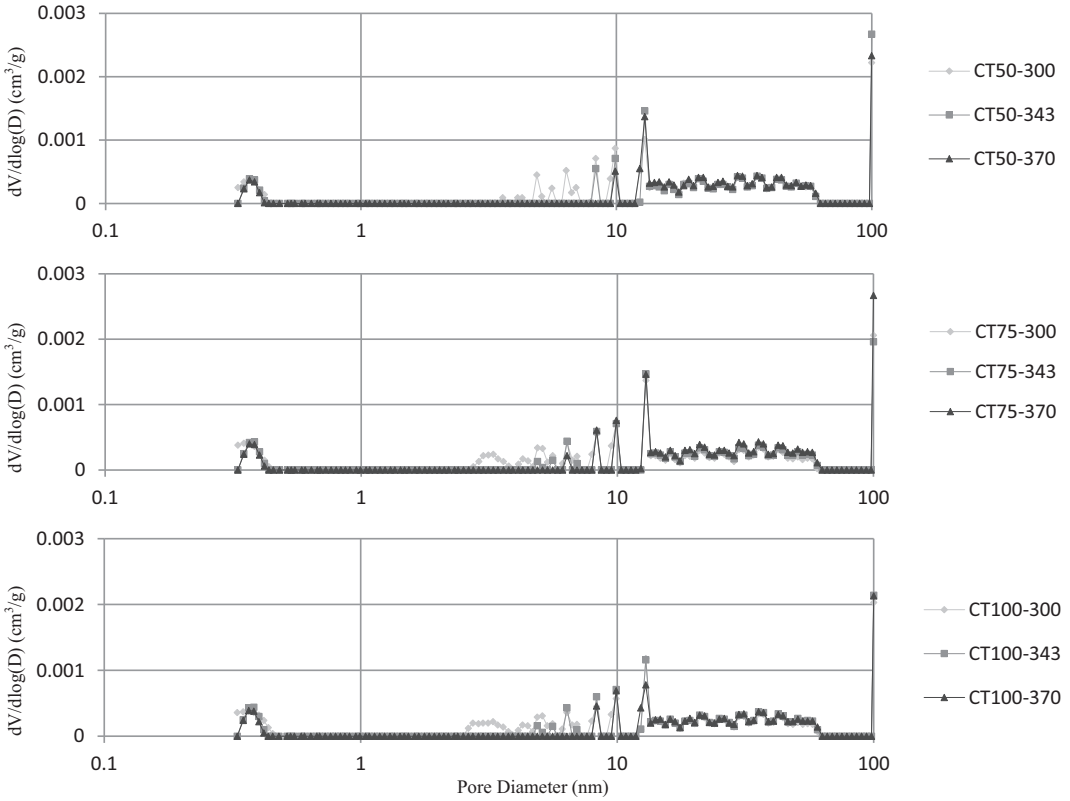

Fig. 4. Plot of dV/dlog(W) versus Pore diameter for the thermally evolved solid residues of the investigated shale after extration at various conditions.

Table 3
The pore structure parameters (surface areas, pore volumes) for original shale and its thermally evolved solid residues at various conditions.

	TOC (%)	N_2			CO_2		$N_2 + CO_2$	
		S_{BET} (m^2/g)	V_{BJH} (10^{-3} cm^3/g)	D_{BET} (nm)	S_{D-R} (m^2/g)	V_{D-A} (10^{-3} cm^3/g)	S_{NLDFT} (m^2/g)	V_{NLDFT} (10^{-3} cm^3/g)
Original	5.39	16.42	26.89	6.58	11.96	6.97	21.27	26.88
50–300	5.74	3.74	17.86	15.72	14.01	12.11	7.92	14.86
50–343	5.51	2.75	18.23	22.09	11.20	9.19	9.45	16.83
50–370	4.96	2.21	14.70	22.03	11.96	7.87	9.10	18.13
75–300	4.93	2.81	18.28	22.19	12.28	11.49	6.46	14.97
75–343	5.05	2.69	16.12	20.98	13.28	14.02	6.15	14.30
75–370	4.93	2.81	18.28	22.19	12.28	11.49	6.46	14.97
100–300	5.53	4.96	18.74	13.59	17.08	15.87	6.20	15.32
100–343	5.03	2.86	17.17	20.67	13.25	13.66	6.04	13.42
100–370	4.7	2.55	16.38	20.88	11.92	9.68	6.32	15.82
EX-original	5.08	17.60	20.74	5.06	11.96	7.87	23.04	21.97
EX-50-300	5.52	5.92	20.27	11.98	15.52	17.74	10.95	21.07
EX-50-343	4.94	3.63	16.20	16.13	14.31	12.02	14.81	14.69
EX-50-370	4.82	2.90	14.18	17.01	12.88	9.04	14.25	12.50
EX-75-300	5.21	9.31	21.51	8.43	18.84	18.46	7.87	21.64
EX-75-343	4.85	4.58	16.39	12.72	16.01	13.96	9.27	14.71
EX-75-370	4.71	4.13	19.27	16.31	14.78	12.28	9.56	17.09
EX-100-300	5.23	8.93	24.05	9.76	19.08	18.09	6.87	19.56
EX-100-343	4.81	4.75	18.11	13.03	16.15	14.14	8.10	15.62
EX-100-370	4.51	3.79	19.10	17.36	15.93	17.50	8.47	16.63

Note: S_{BET} = BET surface area; S_{D-R} = Micropore surface area by D-R method; S_{NLDFT} = Total surface area (0.33–100 nm) by NLDFT method; V_{BJH} = BJH adsorption cumulative volume; V_{D-A} = Limited micropore volume by D-A method; V_{NLDFT} = Total pore volume (0.33–100 nm) by NLDFT method; D_{BET} = BET adsorption average pore diameter.

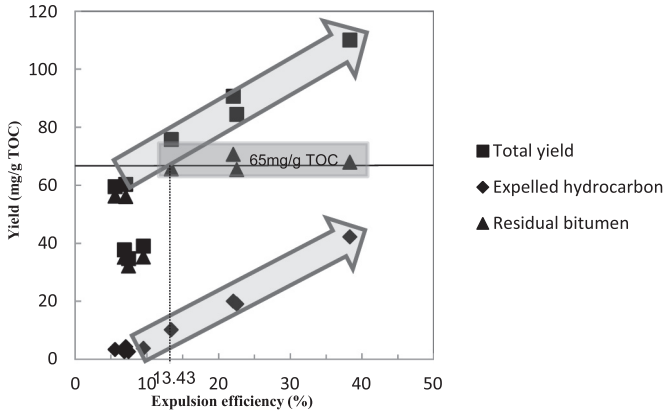

Fig. 5. Plots showing the evolution of the yield of total generated hydrocarbon, expelled hydrocarbon, residual bitumen with increasing expulsion efficiency.

et al., 2017). They all found that the pore volume in extracted shale increased compared to the corresponding original shale (before extraction) in the range of pore diameters from 0 to over 100 nm. However, for most of the investigated samples, only the nanopores with diameters in the range of 1–10 nm increased from solvent extraction (Fig. 6). It was probably because the high pressure pushed the retained hydrocarbon into the nanopores with narrow pore diameters (1–10 nm in this study). Here, all of the shale samples were subjected to high pressures of 50 MPa–100 MPa and were then analyzed for PSD immediately. In comparison, the samples investigated in most of the previous studies were outcrop shale samples (e.g., Mastalerz et al., 2013; Valenza et al., 2013; Wei et al., 2014; Zargari et al., 2015; Zhang et al., 2017). For such samples, the retained hydrocarbons may gradually return to the nanopores with diameters larger than 10 nm because the lithostatic pressure from the overlying strata is released when they are uplifted to the surface. This implies that for natural shale gas plays that are very deep below the surface, most of the retained hydrocarbons probably occupied pores with very narrow diameters due to high pressure.

Meanwhile, it seems from Fig. 6 that Soxhlet extraction does not always increase the volume of nanopore. A decline in mesopore volumes was also found in some experiments, such as at 300 °C and 75 MPa (Fig. 6B) and at 343 °C and 100 MPa (Fig. 6F). A similar change was also reported by Wei et al. (2014), who did not observe an increase in mesopore volumes of four unextracted New Albany shale samples (60 mesh fractions) from Indiana and Illinois with Ro from 0.55% to 1.41% compared to those observed after extraction with different solvents (DCM, toluene). Since only the pore diameters of 0.33–100 nm are discussed in this study, the decline in mesopore volumes of unextracted samples compared to extracted samples was probably because the mesopore space was enlarged to the macropore range by the extraction of clogged oil/bitumen (Wei et al., 2014). Furmann et al. (2013) also reported the decline of BET surface areas and mesopore volumes for an unextracted high volatile bituminous coal (Ro = 0.69%) compared to the corresponding DCM extracted coal. They also suggest the decline of BET surface areas and mesopore volumes was due to progressive opening of larger pores.

Fig. 7 shows the evolution of pore volume (0-10 nm) in relation to the expulsion efficiency and the variation in residual bitumen content in relation to the expulsion efficiency. The volumes of retained hydrocarbons were calculated by assuming that the density of generated hydrocarbon is 0.9 g/cm^3. When EE was lower than 13.43%, the volumes of micropores plus fine mesopores were reduced, but the volume of retained hydrocarbons increased with increasing EE. Meanwhile, the volume of micropores plus fine mesopores was sufficiently large for the storage of retained hydrocarbons with EE < 13.43% (Fig. 7. and Table 4). However, when EE was higher than 13.43%, the volumes for both retained hydrocarbons and micropores plus fine mesopores were stable with a further increase in EE, and the volume of retained hydrocarbons was in excess of the volume of micropores plus fine mesopores (Fig. 7. and Table 4). The extra retained hydrocarbons probably stayed in nanopores with diameters > 10 nm and/or absorbed into the macrostructure of the residual kerogen.

4.3. The effect of oil expulsion on pore size distribution (PSD)

The evolution of nanopores in shale is very important for evaluating reservoir quality and hydrocarbon potential (Loucks et al., 2009; Jarvie, 2012; Curtis et al., 2012). Here, the influence of oil expulsion on pore

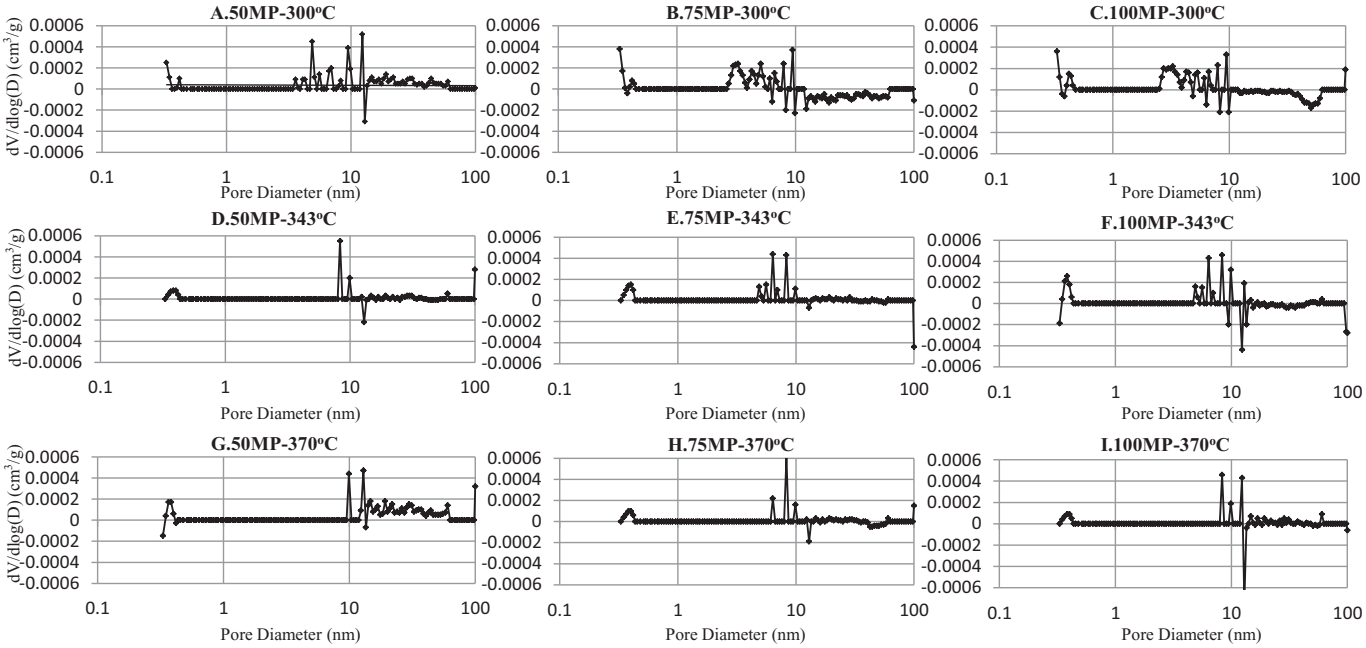

Fig. 6. Plot of dV/dlog(D) versus D for the difference of pore size distribution between the pyrolyzed shale after Soxhlet extraction and that before Soxhlet extraction at various conditions.

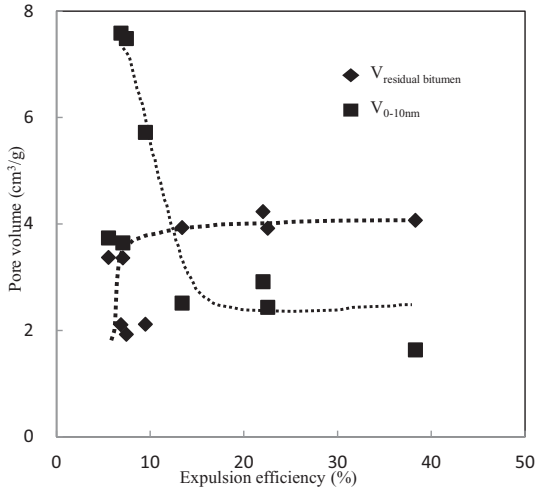

Fig. 7. Plots showing the evolution of volume of residual bitumen and pore with diameter of 0–10 nm with increasing expulsion efficiency.

structure distribution was discussed.

Fig. 8 shows the relationship between the pore volume of nanopore with different pore diameters and the increasing EE. A negative correlation was observed between EE and the pore volumes for micro- and fine mesopores (Fig. 8A and B). However, there was no obvious correlation between the EE and the pore volumes for medium mesopores, coarse mesopores and macropores (Fig. 8C–F). Meanwhile, it seemed that the varying trend of pore volumes for micropores and fine mesopores with EE can be divided into two stages. The pore volumes for micropores and fine mesopores decreased sharply in the first stage (EE < 13.43%), whereas they decreased slowly in the second stage (EE > 13.43%). Interestingly, the EE of 13.43% was also the critical point for the amount of hydrocarbon retention (Fig. 5), implying that the evolution of pore volumes for micropores and fine mesopores (D < 10 nm) is related to hydrocarbon retention. It also further confirmed the above conclusion that most of the retained hydrocarbons in the investigated samples probably occupied pores with very narrow diameters (1–10 nm).

To further discuss the influence of oil expulsion on the evolution of micropore and fine mesopore volumes, the relationships among the expelled hydrocarbon, residual bitumen, total generated hydrocarbon and the micropore and fine mesopore volume were correlated in Fig. 9. It seems the amount of expelled hydrocarbon, residual bitumen, and total generated hydrocarbon all show negative correlation with the micropore and fine mesopore volume. That means that the reduction of micropores and fine mesopores in shale may be related to the increase of expelled hydrocarbon, residual bitumen, or total generated

Table 4
The pore volumes for different range of pore and the volume of residual bitumen in the pyrolyzed shales at various conditions.

Temperature (°C)	Pressure (MPa)	$V_{micropore}$ (10^{-3} cm³/g)	$V_{fine\ mesopore}$ (10^{-3} cm³/g)	$V_{medium\ mesopore}$ (10^{-3} cm³/g)	$V_{coarse\ mesopore}$ (10^{-3} cm³/g)	$V_{macropore}$ (10^{-3} cm³/g)	$V_{residual\ bitumen}$ (10^{-3} cm³/g)
300	50	1.70	4.02	6.60	5.09	3.66	2.11
	75	2.03	5.45	5.93	4.76	3.47	1.92
	100	2.20	5.38	4.72	4.04	3.22	2.10
343	50	1.25	1.26	5.09	4.08	3.01	3.93
	75	1.48	2.16	4.56	3.65	2.86	3.35
	100	1.52	2.21	4.69	3.99	3.21	3.36
370	50	1.12	0.51	4.46	3.62	2.79	4.06
	75	1.32	1.59	5.52	4.74	3.92	4.23
	100	1.28	1.15	5.41	4.83	3.96	3.91

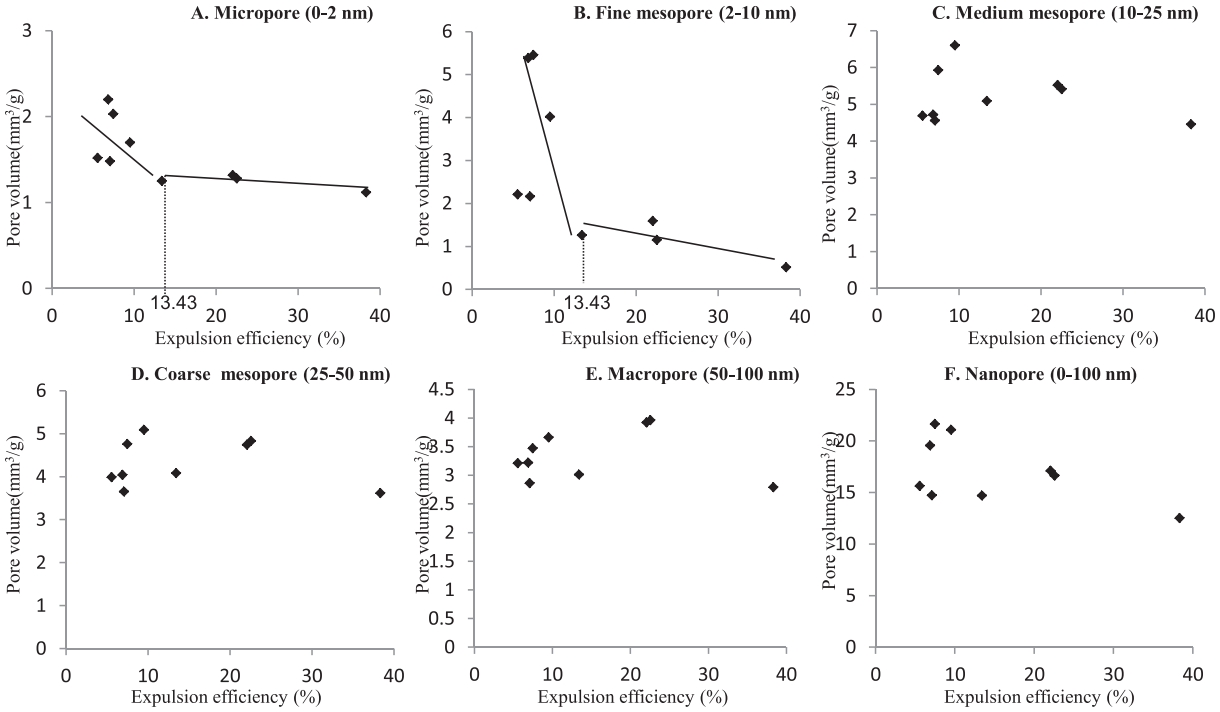

Fig. 8. Plots showing the relationships of expulsion efficiency with pore volume of micropore (A), fine mesopore (B), medium mesopore (C), coarse mesopore (D), macropore (E), and nanopore with diameter of 0–100 nm (F).

hydrocarbon. However, the relationship of the micropore and fine mesopore volumes with expelled hydrocarbon (Fig. 9 Aa and Ab) is most similar to the relationship of the micropore and fine mesopore volumes with EE (Fig. 8 A and B). This indicates that the increase of expelled hydrocarbon (rather than residual bitumen or total generated hydrocarbon) is the dominating factor controlling the reduction of micropores and fine mesopores in shale. Meanwhile, the hydrocarbon was expelled from occupied sites in source rocks (micropores and mesopores in this study) by the force of pressure. Additionally, sediments progressively lose their porosity due to the loading pressure (compaction effect). Thus, the reduction of micropores and fine mesopores was probably because their compaction was associated with the expulsion of hydrocarbon within shale.

The micropore and fine mesopore volumes also decreased with increasing residual bitumen (Fig. 9 Ba and Bb), implying that the pore volumes were much larger than the volumes of retained bitumen

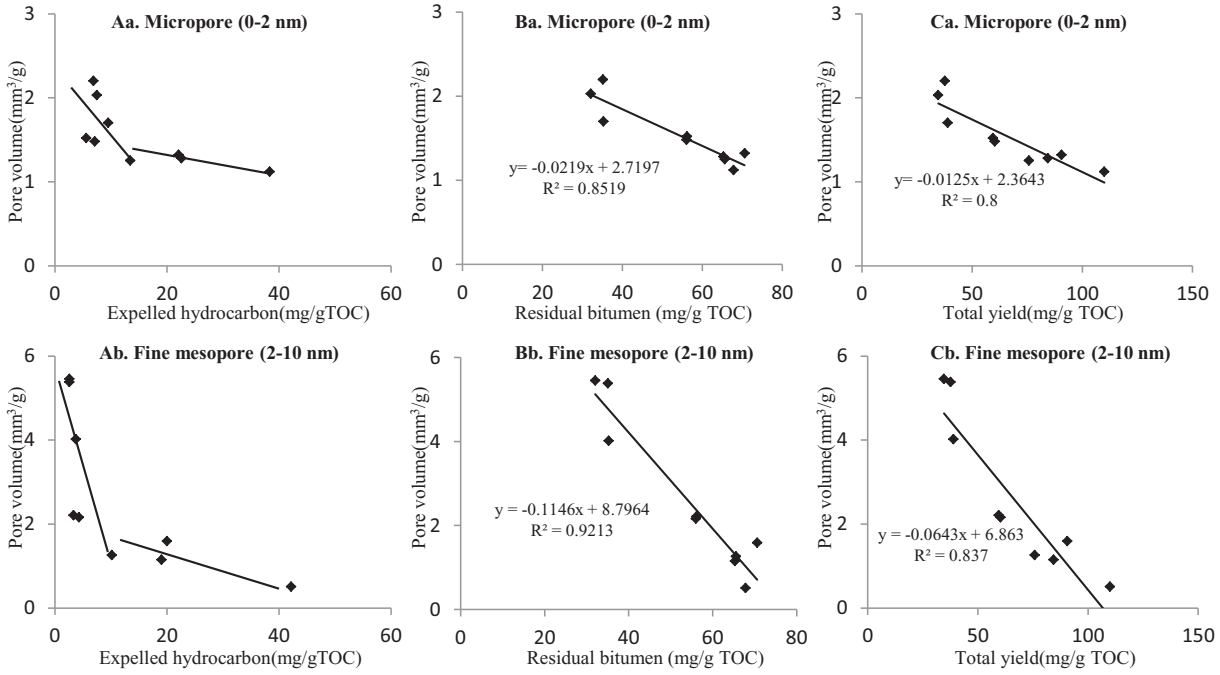

Fig. 9. Plots showing the relationships of pore volume of micropore, fine mesopore with expulsion efficiency (Aa, Ab), the amount of residual bitumen (Ba, Bb), the amount of total generated hydrocarbons (Ca, Cb).

(Fig. 7). However, when the amount of retained hydrocarbon reached the saturation threshold yield of 65 mg/g TOC, the micropore and fine mesopore volumes did not decline. It seems the maintenance effect of retained oil resists further pore volume reduction from compaction. Additionally, the pore volume decline rates for micropores versus residual bitumen and total yield were much lower than those for the fine mesopore volume (Fig. 9 Ba, Bb, Ca, Cb), indicating that fine mesopores are easier to reduce than micropores which is consistent with the results of previous studies (Mastalerz et al., 2013; Liu et al., 2017).

4.4. The oil expulsion model and its implications for evaluating shale gas plays

There are many models to explain the physical and chemical processes of oil expulsion within source rocks. Some believe that oil expulsion occurs when the generated hydrocarbons exceed a saturation threshold due to the absorption (physical) and adsorption (chemical) properties of organic matter in the source rocks (e.g., Durand, 1988; Lafargue et al., 1994; Ritter, 2003). Other researchers have suggested that the pressure buildup from generation, compaction and the framework collapse of the rock fabric microstructure are key factors in oil expulsion (e.g., Barker, 1972; Hunt, 1990). However, for the investigated shale, oil expulsion seemed to be controlled by both the pressure-driving and the absorption-adsorption mechanisms. The oil expulsion process for the investigated shale can be divided into two stages. In the first stage (Easy %Ro < 1.0, EE < 13.43%), though the amounts of total generated hydrocarbon (32.05–56.16 mg/g TOC in Table 2) are lower than the saturation threshold value (65 mg/g TOC), expelled hydrocarbons (2.59–4.27 mg/g TOC) can still be observed. Such expelled hydrocarbons were probably driven by the compaction of micropores and fine mesopores. However, when the amount of generated hydrocarbons was over the saturation threshold (Easy %Ro: 1.0%–1.3%, EE > 13.43% in this study), the absorption-adsorption mechanism will dominantly controlled oil expulsion.

Meanwhile, oil expulsion has a different influence on the evolution of nanopores in the abovementioned two evolution stages. In the early stage of oil expulsion (EE < 13.43%), the volume of micropores and fine mesopores will gradually reduce with increasing pressure and temperature, because the nanopore volume is sufficiently large to store retained hydrocarbon at the beginning of oil expulsion. Meanwhile, the amount of retained oil increases gradually with increasing pressure and temperature. For the investigated shale, the volume of retained oil finally surpassed the sum of micropore and fine mesopore volumes when the saturation threshold was reached (EE = 13.43%). When the volume of retained oil is over the sum of micropore and fine mesopore volumes (EE ≥ 13.43%), the reduction rate of micropores and fine mesopores versus EE decreases sharply, because the maintenance effect of the retained oil will resist the compaction effect of pressure.

The retention of hydrocarbon in shale has a very important role in shale oil and gas potential. Generally, low oil expulsion efficiency will cause a high amount of retarded hydrocarbon in shale. Thus, low oil expulsion efficiency will benefit the formation of shale oil and gas. In fact, most of the commercial shale gas plays have low oil expulsion efficiency (Jarvie, 2012). Based on this study, it seems the maximum amount of retained hydrocarbon within shale was mostly controlled by the threshold of saturation absorption. It indicated that source rocks with high total organic carbon (TOC) are beneficial for oil retention and the formation of shale gas. It was also confirmed by previous research on natural maturity sequences (Tian et al., 2015; Zargari et al., 2015; Han et al., 2015), which suggested that the TOC content exerts a major control on hydrocarbon retention. Meanwhile, although clays also have sorptive properties for oil, the adsorption on clay appears to be of less importance for hydrocarbon retention (Espitalie et al., 1980; Schettler and Parmely, 1991), probably because of clay mineral dehydration and framework collapse during thermal maturation (Bray et al., 1998; Bala et al., 2000; Neanman et al., 2003; Noyan et al., 2006).

5. Conclusions

In this study, semi-closed pyrolysis was conducted on a shale sample to simulate its generation and expulsion processes of shale oil or gas. The results revealed that oil expulsion of shale can be divided into two stages. In the first stage (Easy %Ro < 1.0% and EE < 13.43%), the primary driving force for oil expulsion was compaction from overlying lithostatic pressure. Meanwhile, most of the generated oil will be pushed into nanopores with diameters < 10 nm by pressure. Thus, during the initial period, the expulsion of oil will lead to the reduction of micropore and fine mesopore volumes (D < 10 nm). With a further increasing pressure and temperature (Easy %Ro: 1.0%–1.3% and EE > 13.43%), most of the micropores and fine mesopores will finally be compacted, and the amount of generated hydrocarbon will be over the maximum absorbed value of kerogen. At this stage (EE > 13.43% in this study), the influence of oil expulsion on the micropores and fine mesopores was sharply reduced due to the maintenance effect of retained hydrocarbons on the pore system. This study also confirmed that the amount of retained hydrocarbon within shale is controlled by the threshold of saturation absorption rather than pressure in the oil-generative window.

Acknowledgements

This work was supported by the Strategic Priority Research Program of the Chinese Academy of Sciences (Class B) (Grant No. XDB10010502). We would like to acknowledge Master Shuhuan Ji and Xinyan Fang for laboratory assistance. We are grateful to Editor-in-chief Dr. Cevat Özgen Karacan and anonymous reviewer for their instructive comments and suggestions that significantly help clarify this manuscript. This is contribution No.IS-2521 from GIGCAS.

References

Bala, P., Samantaray, B.K., Srivastava, S.K., 2000. Behydration transformation in Ca-montmorillonite. Bull. Mar. Sci. 23, 61–67.
Barker, C., 1972. Aquathermal pressuring: role of temperature in development of abnormal-pressure zones. AAPG Bull. 56, 2068–2071.
Bray, H., Redfern, S.A.T., Clark, S.M., 1998. The kinetics of dehydration in Ca-montmorillonite: an in situ X-ray diffraction study. Mineral. Mag. 62, 647–656.
Cao, T.T., Song, Z.G., Wang, S.B., Cao, X.X., Li, Y., Xia, J., 2015. Characterizing the pore structure in the Silurian and Permian shales of the Sichuan Basin, China. Mar. Pet. Geol. 61, 140–150.
Chalmers, G.R., Bustin, R.M., Power, I.M., 2012. Characterization of gas shale pore systems by porosimetry, pycnometry, surface area, and field emission scanning electron microscopy/transmission electron microscopy image analyses: examples from the Barnett, Woodford, Haynesville, Marcellus, and Doig units. AAPG Bull. 96, 1099–1119.
Chen, J., Xiao, X.M., 2014. Evolution of nanoporosity in organic-rich shales during thermal maturation. Fuel 129, 173–181.
Chen, S.B., Zhu, Y.M., Wang, H.Y., Liu, H.L., Wei, W., Fang, J.H., 2011. Shale gas reservoir characterization: a typical case in the southern Sichuan Basin of China. Energy 36, 6609–6616.
Curtis, J.B., 2002. Fractured shale-gas systems. AAPG Bull. 86, 1921–1938.
Curtis, M.E., Cardott, B.J., Sondergeld, C.H., Rai, C.S., 2012. Development of organic porosity in the Woodford Shale with increasing thermal maturity. Int. J. Coal Geol. 103, 26–31.
Dai, J.X., Ni, Y.Y., Gong, D.Y., Feng, Z.Q., Liu, D., Peng, W.L., Han, W.X., 2017. Geochemical characteristics of gases from the largest tight sand gas field (Sulige) and shale gas field (Fuling) in China. Mar. Pet. Geol. 79, 426–438.
Durand, B., 1988. Understanding of HC migration in sedimentary basins (present state of knowledge). Org. Geochem. 13, 445–459.
Espitalie, J., Madec, M., Tissot, B., 1980. Role of mineral matrix in kerogen pyrolysis: influence on petroleum generation and migration. AAPG Bull. 64, 59–66.
Furmann, A., Mastalerz, M., Brassell, S.C., Schimmelmann, A., Picardal, F., 2013. Extractability of biomarkers from high- and low-vitrinite coals and its effect on the porosity of coal. Int. J.Coal Geol. 107, 141–151.
Groen, J.C., Peffer, L.A.A., Perez-Ramírez, J., 2003. Pore size determination in modified micro- and mesoporous materials. Pitfalls and limitations in gas adsorption data analysis. Microporous Mesoporous Mater. 60, 1–17.
Han, Y.J., Mahlstedt, N., Horsfield, B., 2015. The Barnett sahle: compositional fractionation associated with intraformational petroleum migration, retention, and expulsion. AAPG Bull. 99, 2173–2202.
Hunt, J.M., 1990. Generation and migration of petroleum from abnormally pressured fluid compartments. AAPG Bull. 74, 1–12.

Jarvie, D.M., 2012. Shale resource systems for oil and gas: Part 1–shale-gas resource systems. AAPG Mem. 97, 89–119.
Jarvie, D.M., Hill, R.J., Ruble, T.E., Pollastro, R.M., 2007. Unconventional shale-gas systems: the Mississippian Barnett Shale of north-central Texas as one model for thermogenic shale-gas assessment. AAPG Bull. 91, 475–499.
Jin, X.D., Li, E.T., Pan, C.C., Yu, S., Liu, J.Z., 2013. Interaction of coal and oil in confined pyrolysis experiments: insight from the yield and composition of gas hydrocarbons. Mar. Pet. Geol. 48, 379–391.
Lafargue, E., Espitalié, J., Broks, T., Jacobsen, T., Nyland, B., 1994. Experimental simulation of primary migration. Org. Geochem. 22, 575–586.
Liu, B.Q., Cai, B., Fang, J., 1990. A simulation experiment of petroleum origin on kerogen from shales of the Xiamaling formation in the upper Proterozoic. Exper. Petrol. Geol. 12, 147–161.
Liu, S., Yong-Sheng, M.A., Cai, X., Guo-Sheng, X., Wang, G., Yong, Z., Wei, S., Yuan, H., 2009. Characteristic and accumulation process of the natural gas from sinian to lower paleozoic in Sichuan Basin, China. J. Chengdu Univ. Technol. 36 (4), 345–354.
Liu, Y.K., Xiong, Y.Q., Li, Y., Peng, P.A., 2017. Effects of oil expulsion and pressure on nanopore development in highly mature shale: evidence from a pyrolysis study of the Eocene Maoming oil shale, south China. Mar. Pet. Geol. 86, 526–536.
Loucks, R.G., Reed, R.M., Ruppel, S.C., Jarvie, D.M., 2009. Morphology, genesis, and distribution of nanometer-scale pores in siliceous mudstones of the Mississippian Barnett Shale. J. Sediment. Res. 79, 848–861.
Lu, J.L., 1990. The modelling experiment of coal-generated hydrocarbons. In: Fu, J., Liu, D., Sheng, G. (Eds.), Geochemistry of Coal-generated Hydrocarbons. Science Press, Beijing, China, pp. 40–46.
Ma, Y.S., Zhang, S.C., Guo, T.L., Zhu, G.Y., Cai, X.Y., Li, M.W., 2008. Petroleum geology of the Puguang sour gas field in the Sichuan Basin, SW China. Mar. Pet. Geol. 25 (4–5), 357–370.
Mastalerz, M., Drobniak, A., Strąpoć, D., Solano Acosta, W., Rupp, J., 2008. Variations in pore characteristics in high volatile bituminous coals: implications for coalbed gas content. Int. J. Coal Geol. 76, 205–216.
Mastalerz, M., Schimmelmann, A., Drobniak, A., Chen, Y., 2013. Porosity of Devonian and Mississippian New Albany Shale across a maturation gradient: insights from organic petrology, gas adsorption, and mercury intrusion. AAPG Bull. 97, 1621–1643.
Mathia, E.J., Bowen, L., Thomas, K.M., Aplin, A.C., 2016. Evolution of porosity and pore types in organic-rich, calcareous, Lower Toarcian Posidonia Shale. Mar. Pet. Geol. 75, 117–139.
Michels, R., Landais, P., 1994. Effects of pressure on organic matter maturation during confined pyrolysis of Woodford kerogen. Energy Fuel 8, 741–754.
Modica, C.J., Lapierre, S.G., 2012. Estimation of kerogen porosity in source rocks as a function of thermal transformation: example from the Mowry Shale in the Powder River Basin of Wyoming. AAPG Bull. 96, 87–108.
Montgomery, S.L., Jarvie, D.M., Bowker, K.A., Pollastro, R.M., 2005. Mississippian Barnett shale, fort Worth Basin, north-central Texas: gas-shale play with multitrillion cubic foot potential. AAPG Bull. 89, 155–175.
Neanman, A., Pelletier, M., Villieras, F., 2003. The effects of exchanged cation, compression, heating and hydration on textural properties of bulk bentonite and its corresponding purified montmorillonite. Appl. Clay Sci. 22, 153–168.
Noyan, H., Onal, M., Sarikaya, Y., 2006. The effect of heating on the surface area, porosity and surface acidity of a bentonite. Clay Clay Miner. 54, 375–381.
Pan, C.C., Jiang, L.L., Liu, J.Z., Zhang, S.C., Zhu, G.Y., 2012. The effects of pyrobitumen on oil cracking in confined pyrolysis experiments. Org. Geochem. 45, 29–47.
Pepper, A.S., Corvi, P.J., 1995. Simple kinetic models of petroleum formation. Part III: modelling an open system. Mar. Pet. Geol. 12, 417–452.
Pollastro, R.M., 2007. Total petroleum system assessment of undiscovered resources in the giant Barnett Shale continuous (unconventional) gas accumulation, Fort Worth Basin, Texas. AAPG Bull. 91, 551–578.
Ritter, U., 2003. Fractionation of petroleum during expulsion from kerogen. J. Geochem. Explor. 78–79, 417–420.
Ross, D.J.K., Bustin, R.M., 2007. Shale gas potential of the lower Jurassic Gordondale Member, northeastern British Columbia, Canada. Bull. Can. Pet. Geol. 77, 51–75.
Ross, D.J.K., Bustin, R.M., 2008. Characterizing the shale gas resource potential of Devonian-Mississippian strata in the Western Canada Sedimentary Basin: application of an integrated formation evaluation. AAPG Bull. 92, 87–125.
Sandvik, E.I., Young, W.A., Curry, D.J., 1992. Expulsion from hydrocarbon sources: the role of organic absorption. Org. Geochem. 19, 77–87.
Schettler Jr., P.D., Parmely, C.R., 1991. Contributions to total storage capacity in Devonian shales. In: SPE Eastern Regional Meeting, Lexington, Kentucky, October 22–25, 1991, SPE Paper 23422, pp. 77–88.
Sing, K.S., Everett, D.H., Haul, R.A.W., Moscou, L., Pierotti, R.A., Rouquerol, J., Siemieniewsha, T., 1985. Reporting physisorption data for gas/solid systems with special reference to the determination of surface area and porosity. Pure Appl. Chem. 57, 603–619.
Stainforth, J.G., Reinders, J.K.A., 1990. Primary migration of hydrocarbons by diffusion through organic matter networks, and its effect on oil and gas generation. Org. Geochem. 16, 61–74.
Suárez-Ruiz, I., Juliao, T., Suárez-García, F., Marquez, R., Ruiz, B., 2016. Porosity development and the influence of pore size on the CH_4 adsorption capacity of a shale oil reservoir (Upper Cretaceous) from Colombia. Role of solid bitumen. Int. J. Coal. Geol. 159, 1–17.
Sun, W., Liu, S., Ran, B., Wang, S., Yue-Hao, Y.E., Luo, C., 2012. General situation and prospect evaluation of the shale gas in Niutitang formation of Sichuan Basin and its surrounding areas. J. Chengdu Univ. Technol. 39 (2), 170–175.
Sun, L.N., Tuo, J.C., Zhang, M.F., Wu, C.J., Wang, Z.X., Zheng, Y.W., 2015. Formation and development of the pore structure in Chang 7 member oil-shale from Ordos Basin during organic matter evolution induced by hydrous pyrolysis. Fuel 158, 549–557.
Sweeney, J.J., Burnham, A.K., 1990. Evaluation of a simple method of vitrinite reflectance based on chemical kinetics. AAPG Bull. 74, 1559–1570.
Tan, J., Horsfield, B., Fink, R., Krooss, B., Schulz, H.M., Rybacki, E., Zhang, J., Boreham, C.J., Graas, G.V., Tocher, B.A., 2014. Shale gas potential of the major marine shale formations in the upper Yangtze platform, south China, part III: mineralogical, lithofacial, petrophysical, and rock mechanical properties. Energy Fuel 28 (4), 2322–2342.
Tang, X., Zhang, J.C., Jin, Z.J., Xiong, J.Y., Lin, L.M., Yu, Y.X., Han, S.B., 2015. Experimental investigation of thermal maturation on shale reservoir properties from hydrous pyrolysis of Chang 7 shale, Ordos Basin. Mar. Pet. Geol. 64, 165–172.
Thomas, M.M., Clouse, J.A., 1990a. Primary migration by diffusion through kerogen: I. Model experiments with organic-coated rocks. Geochim. Cosmochim. Acta 54, 2775–2779.
Thomas, M.M., Clouse, J.A., 1990b. Primary migration by diffusion through kerogen: II. Hydrocarbon diffusivities in kerogen. Geochim. Cosmochim. Acta 54, 2781–2792.
Thomas, M.M., Clouse, J.A., 1990c. Primary migration by diffusion through kerogen: III. Calculation of geologic fluxes. Geochim. Cosmochim. Acta 54, 2793–2797.
Thommes, M., Kaneko, K., Neimark, A.V., Olivier, J.P., Rodriguezreinoso, F., Rouquerol, J., Sing, K.S.W., 2015. Physisorption of gases, with special reference to the evaluation of surface area and pore size distribution (IUPAC technical report). Pure Appl. Chem. 87 (9), 25.
Tian, H., Pan, L., Zhang, T.W., Xiao, X.M., Meng, Z.P., Huang, B.J., 2015. Pore characterization of organic-rich lower Cambrian shales in Qiannan depression of Guizhou Province, Southwestern China. Mar. Pet. Geol. 62, 28–43.
Tissot, B.P., Welte, D.H., 1984. Petroleum Formation and Occurrence, 2nd ed. Springer-Verlag, Berlin, pp. 1–699.
Valenza, J.J., Drenzek, N., Marques, F., Pagels, M., Mastalerz, M., 2013. Geochemical controls on shale microstructure. Geology 41, 611–614.
Wang, S.B., Song, Z.G., Cao, T.T., Song, X., 2013. Themethane sorption capacity of Paleozoic shales from the Sichuan Basin, China. Mar. Pet. Geol. 44, 112–119.
Wei, L., Mastalerz, M., Schimmelmann, A., Chen, Y.Y., 2014. Influence of Soxhlet-extractable bitumen and oil on porosity in thermally maturing organic-rich shales. Int. J. Coal Geol. 132, 38–50.
Wei, M.M., Xiong, Y.Q., Zhang, L., Li, J.H., Peng, P.A., 2016. The effect of sample particle size on the determination of pore structure parameters in shales. Int. J. Coal Geol. 163, 177–185.
Wu, K., Ma, Q.F., Feng, Q.L., 2012. Middle Permian pore characteristics and shale gas exploration significance from the Gu-feng Formation in Jian shi, Western Hubei. Earth Sci. J. China. Univ. Geosci. 37, 175–183.
Xiao, X.M., Song, Z.G., Zhu, Y.M., Hui, T., Yin, H.W., 2013. Summary of shale gas research in North American and revelations to shale gas exploration of Lower Paleozoic strata in China south area. J. China Coal Soc. 38 (5), 721–727.
Xie, L.J., Sun, Y.G., Yang, Z.W., Chen, J.P., Jiang, A.Z., Zhang, Y.D., Deng, C.P., 2013. Evaluation of hydrocarbon generation of the Xiamaling Formation shale in Zhangjiakou and its significance to the petroleum geology in North China. Sci. China Earth Sci. 56, 444–452.
Zargari, S., Canter, K.L., Prasad, M., 2015. Porosity evolution in oil-prone source rocks. Fuel 153, 110–117.
Zhang, J.C., Nie, H.K., Bo, X.U., Jiang, S.L., Zhang, P.X., Wang, Z.Y., 2008. Geological condition of shale gas accumulation in Sichuan Basin. Nat. Gas Ind. 28 (2), 151–156.
Zhang, L., Xiong, Y.Q., Li, Y., Wei, M.M., Jiang, W.M., Lei, R., Wu, Z.Y., 2017. DFT modeling of CO_2 and Ar low-pressure adsorption for accurate nanopore structure characterization in organic-rich shales. Fuel 204, 1–11.
Zou, C.N., Dong, D.Z., Wang, Y.M., Li, X.J., Huang, J.L., Wang, S.F., Guan, Q.Z., Zhang, C.C., Wang, H.Y., Liu, H.L., Bai, W.H., Liang, F., Lin, W., Zhao, Q., Liu, D.X., Yang, Z., Liang, P.P., Sun, S.S., Qiu, Z., 2015. Shale gas in China: characteristics, challenges and prospects (II). Pet. Explor. Dev. 42 (6), 753–767.